



**HAL**  
open science

## Influence of the optical system and anatomic points on computer-assisted total knee arthroplasty

Bernard Schlatterer, Jean-Marc Linares, Patrick Chabrand, Jean-Michel Sprael, Jean-Noël Argenson

### ► To cite this version:

Bernard Schlatterer, Jean-Marc Linares, Patrick Chabrand, Jean-Michel Sprael, Jean-Noël Argenson. Influence of the optical system and anatomic points on computer-assisted total knee arthroplasty. *Orthopaedics & Traumatology: Surgery & Research*, 2014, 100, pp.395 - 402. 10.1016/j.otsr.2013.12.029 . hal-01440853

**HAL Id: hal-01440853**

**<https://amu.hal.science/hal-01440853>**

Submitted on 23 Jan 2017

**HAL** is a multi-disciplinary open access archive for the deposit and dissemination of scientific research documents, whether they are published or not. The documents may come from teaching and research institutions in France or abroad, or from public or private research centers.

L'archive ouverte pluridisciplinaire **HAL**, est destinée au dépôt et à la diffusion de documents scientifiques de niveau recherche, publiés ou non, émanant des établissements d'enseignement et de recherche français ou étrangers, des laboratoires publics ou privés.

Original article

# Influence of the optical system and anatomic points on computer-assisted total knee arthroplasty

B. Schlatterer<sup>a,b,\*</sup>, J.-M. Linares<sup>a</sup>, P. Chabrand<sup>a</sup>, J.-M. Sprauel<sup>a</sup>, J.-N. Argenson<sup>a,c</sup>

<sup>a</sup> Aix-Marseille Université, CNRS, ISM UMR 7287, 13288 Marseille cedex 09, France

<sup>b</sup> Institut Monégasque de Médecine et Chirurgie du Sport, 98000 Monaco, Monaco

<sup>c</sup> Institut du Mouvement et de l'Appareil Locomoteur, Hôpital Sainte-Marguerite, CHU Marseille, 13274 Marseille, France

Keywords:

Total knee arthroplasty Navigation

Computer-assisted surgery Anatomic landmarks

**Background:** For over a decade, computer-assisted orthopaedic surgery for total knee arthroplasty has been accepted as ensuring accurate implant alignment in the coronal plane.

**Hypothesis:** We hypothesised that lack of accuracy in skeletal landmark identification during the acquisition phase and/or measurement variability of the infrared optical system may limit the validity of the numerical information used to guide the surgical procedure.

**Methods:** We built a geometric model of a navigation system, with no preoperative image acquisition, to simulate the stages of the acquisition process. Random positions of each optical reflector center and anatomic acquisition point were generated within a sphere of predefined diameter. Based on the virtual geometric model and navigation process, we obtained 30,000 simulations using the Monte Carlo statistical method then computed the variability of the anatomic reference frames used to guide the bone cuts. Rotational variability ( $\alpha$ ,  $\beta$ ,  $\gamma$ ) of the femoral and tibial landmarks reflected implant positioning errors in flexion-extension, valgus-varus, and rotation, respectively. **Results:** Taking into account the uncertainties pertaining to the 3D infrared optical measurement system and to anatomic point acquisition, the femoral and tibial landmarks exhibited maximal alpha (flexion-extension), beta (valgus-varus), and gamma (axial rotation) errors of 1.65° (0.9°); 1.51° (0.98°), and 2.37° (3.84°), respectively. Variability of the infrared optical measurement system had no significant influence on femoro-tibial alignment angles.

**Conclusion:** The results of a Monte Carlo simulation indicate a certain level of vulnerability of navigation systems for guiding position in rotation, contrasting with robustness for guiding sagittal and coronal alignments.

Level of evidence: Level IV.

## 1. Introduction

For over three decades, the correct positioning of total knee arthroplasty (TKA) components has relied on conventional ancillary systems involving intra-medullary or extra-medullary guides. With these systems, bone cut guides are positioned, with a variable degree of accuracy [1–4]. Patient-specific guides may hold promise for the future but have not been proven sufficiently accurate to warrant their use as a reference procedure [5–9]. Computer-assisted orthopaedic surgery was introduced over 10 years ago and has been found to improve implant position accuracy in the coronal plane compared to conventional instrumentation [10–16].

Nevertheless, errors related to the infrared optical detection system and to lack of accuracy in anatomic landmark identification by palpation may escape detection [17,18]. Geometric models characterising TKA navigation systems have been developed to allow numerical simulations that incorporate the various stages of the acquisition process.

We hypothesised that navigation system accuracy was potentially compromised by the variability of the optimal measurement system and of the anatomic points identified by the surgeon during the navigation procedure.

## 2. Material and methods

### 2.1. Development of the geometric model

The geometric model of the navigation system (Fig. 1) was patterned after the Praxim Nanostation. It replicates the left skeletal

\* Corresponding author at: Aix-Marseille Université, CNRS, ISM UMR 7287, 13288 Marseille cedex 09, France.

E-mail address: schlattererb@im2s.mc (B. Schlatterer).

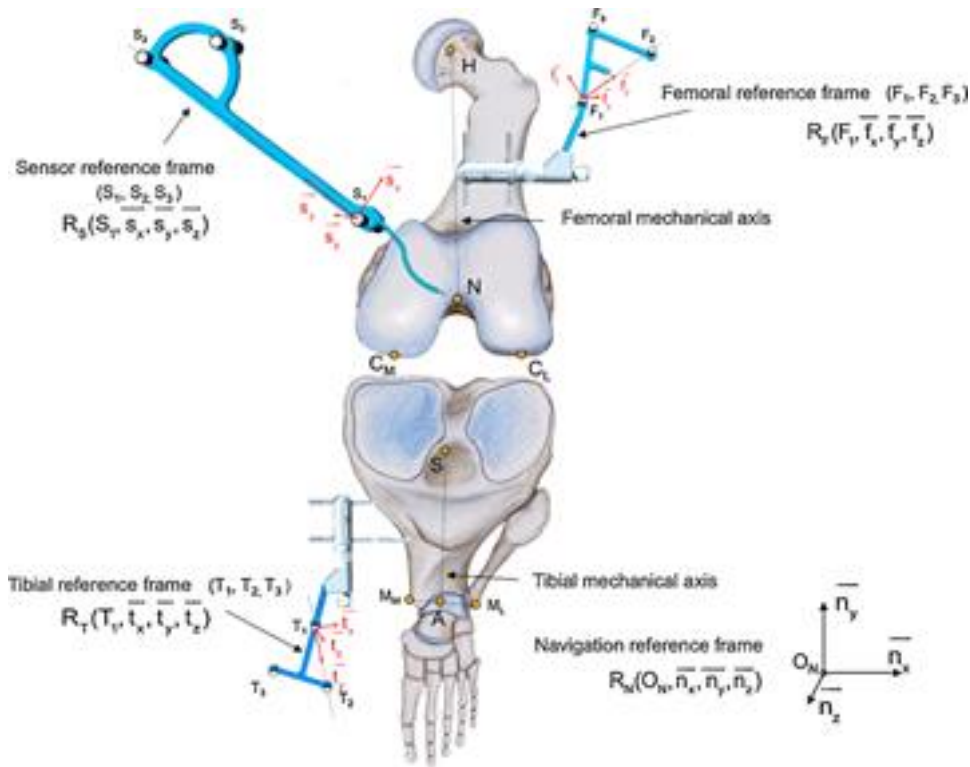


Fig. 1. Frames of references used by the 3D optical measurement system during total knee arthroplasty.

lower limb of a patient installed in the operating room, after surgical exposure of the knee and positioning of the femoral and tibial frames of reference. Tables 1a and 1b list the variables and anatomical measures used. The femoral ('F' shape) and tibial ('T' shape) rigid bodies were assumed to be each secured to the skeleton by two Hoffman-type bicortical external fixators, each equipped with an orientable connector allowing the rigid body to be positioned then fixed in front of the camera.

## 2.2. Construction of the skeletal frames of reference

Each frame of reference comprised three reflective optical trackers attached to a titanium rigid body. The landmarks related to each frame of reference were determined based on three separate geometric points, located at the centres of the three reflective optical trackers on each rigid body (Fig. 2). For example, the  $R_T$  frame of reference associated with the tibia was composed of three orthogonal unit vectors,  $\vec{t}_x$ ,  $\vec{t}_y$ , and  $\vec{t}_z$ , whose origin was point  $T_1$ .

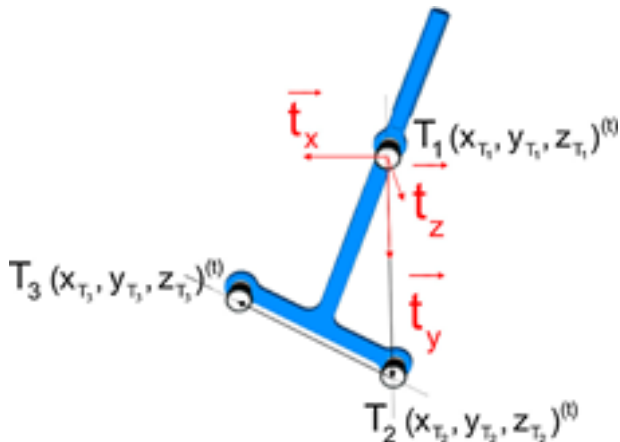


Fig. 2. Construction of the tibial frame of reference.

At each instant, the coordinates of  $\vec{t}_x$ ,  $\vec{t}_y$  and  $\vec{t}_z$  were expressed in the navigator frame of reference  $R_N$  and derived from the coordinates of points  $T_1$  ( $X_{T1}, Y_{T1}, Z_{T1}$ ),  $T_2$  ( $X_{T2}, Y_{T2}, Z_{T2}$ ), and  $T_3$  ( $X_{T3}, Y_{T3}, Z_{T3}$ ), according to the following equations:

$$\vec{t}_y^{(t)}/R_N = \frac{\vec{T}_1 \vec{T}_2}{T_1 T_2}, \quad \vec{t}_z^{(t)}/R_N = \frac{\vec{T}_1 \vec{T}_2 \wedge \vec{T}_1 \vec{T}_3}{T_1 T_2 \wedge T_1 T_3}, \quad \vec{t}_x^{(t)}/R_N = \vec{t}_y^{(t)}/R_N \wedge \vec{t}_z^{(t)}/R_N$$

where  $t$  is the time at computation.

We used the same method for real-time definition of the frames of reference  $R_F$   $F_1, \vec{f}_x, \vec{f}_y, \vec{f}_z$ , and  $R_S$   $S_1, \vec{s}_x, \vec{s}_y, \vec{s}_z$  associated with the femur and mechanical acquisition sensor, respectively, using the centres of the reflective optical trackers ( $F_1, F_2, F_3$ ) and ( $S_1, S_2, S_3$ ).

## 2.3. Modelling of the acquisition phase of the anatomic points

The sequence of acquisition procedures used the three main steps) to compute the coordinates of an acquisition point  $M_i$  as a function of time in each frame of reference. To compute the coordinates of an acquisition point  $M_i$  as a function of time in each frame of reference, the acquisition sequence goes through a three-step procedure. The detailed equations are shown in the [online-only appendix](#).

The second step allowed instantaneous computation of the coordinates of the same acquisition point within the femoral reference frame. The coordinates of  $M_i$  within this local reference frame did not vary with femur position or degree of knee flexion.

The third step consisted in determining the new coordinates of the anatomic point  $M_i$  after each manipulation of the lower limb.

## 2.4. Construction of the anatomical points

The femoral and tibial anatomic points were determined based on the instantaneous positions of all the  $M_i$  anatomic points (Fig. 3).

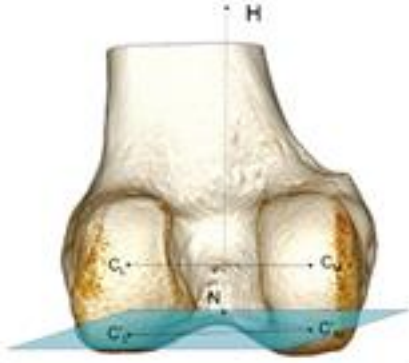
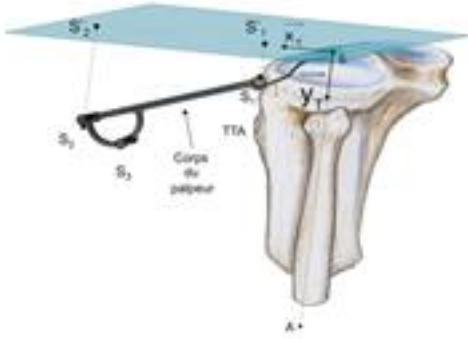
Skeletal landmarks	Construction of the anatomic axis vectors	Comments
$R_f(N, \vec{X}_f, \vec{Y}_f, \vec{Z}_f)$	$\vec{y}_f = \frac{\overline{NH}}{ \overline{NH} }$	The mechanical axis of the femur was defined based on the centre of the femoral head (H) and the centre of the distal femoral epiphysis (N).
	<p>Computation of <math>\vec{C}'_M</math>:</p> $\vec{C}'_M \vec{C}'_M = [\overline{NC_M} \cdot \vec{y}_f] \cdot \vec{y}_f$ <p>The same method was used for <math>\vec{C}'_L</math> with <math>\vec{z}_f = \frac{\overline{C'_L C'_M}}{ \overline{C'_L C'_M} }</math></p> 	To define $\vec{Z}_f$ , the vector $\overline{C'_M C'_L}$ was first projected onto the plan perpendicular to $\vec{y}_f$ , then normalised to yield $\vec{Z}_f$ .
	$\vec{X}_f = \vec{Y}_f \wedge \vec{Z}_f$	
$R_t(S, \vec{X}_t, \vec{Y}_t, \vec{Z}_t)$	$\vec{Y}_t = \frac{\overline{AS}}{ \overline{AS} }$	The two epiphyseal anatomic acquisition points S and A determined the mechanical axis $\vec{Y}_t$ .
	<p>Computation of <math>\vec{S}'_1</math>:</p> $\vec{S}'_1 \vec{S}'_1 = [\overline{SS_1} \cdot \vec{y}_t] \cdot \vec{y}_t$ <p>The same method was used for <math>\vec{S}'_2</math> with</p> $\vec{x}_t = \frac{\overline{S'_1 S'_2}}{ \overline{S'_1 S'_2} }$ 	The sagittal vector $\vec{X}_t$ was acquired by immobilising the navigator sensor with its tip in contact with the surface anterior to the tibial spines and its long axis ( $S_1, S_2$ ) perpendicular to the line connecting the posterior edges of the two tibial plateaux. The two points thus registered, $S_1$ and $S_2$ , were projected onto the plane perpendicular to the mechanical axis to obtain the vector $\vec{X}_t$ perpendicular to $\vec{Y}_t$ .
	$\vec{Z}_t = \vec{X}_t \wedge \vec{Y}_t$	

Fig. 3. Construction of the anatomic landmarks with the acquisition points.

**Table 1a**

Overview of the points and landmarks used to build a geometric model of the navigation system for total knee arthroplasty.

Acquisition of the anatomic points of interest	
Femoral epiphysis	
H	Centre of the femoral head <sup>a</sup>
N	Centre of the distal femoral epiphysis at the highest point of the anterior notch <sup>b</sup>
C <sub>M</sub>	Medial femoral condyle (algorithm)
C <sub>L</sub>	Lateral femoral condyle (algorithm)
C' <sub>M</sub> C' <sub>L</sub>	Orthogonal projection of C <sub>M</sub> C <sub>L</sub> in plane $\rho$ (algorithm)
$\rho_F$	Plane perpendicular to the femoral mechanical axis (algorithm)
Tibial epiphysis	
S	Centre of the proximal tibial epiphysis at the level of surface anterior to the tibial spines <sup>b</sup>
T	Anterior tibial tuberosity <sup>b</sup>
M <sub>M</sub>	Medial malleolus <sup>b</sup>
M <sub>L</sub>	Lateral malleolus <sup>b</sup>
A	Centre of the ankle corresponding to the middle of the M <sub>M</sub> M <sub>L</sub> segment (algorithm)
Reflective infrared optical trackers represented by the corresponding points localized based on their spatial coordinates	
F <sub>1</sub> , F <sub>2</sub> , F <sub>3</sub>	Reflective trackers (3 points) of the femoral frame of reference
T <sub>1</sub> , T <sub>2</sub> , T <sub>3</sub>	Reflective trackers (3 points) of the tibial frame of reference
S <sub>1</sub> , S <sub>2</sub> , S <sub>3</sub>	Reflective trackers (3 points) of the sensor frame of reference
Landmarks for each frame of reference	
R <sub>F</sub> F <sub>1</sub> , $\vec{f}_x$ , $\vec{f}_y$ , $\vec{f}_z$	Landmark for the frame of reference secured to the femur
R <sub>T</sub> T <sub>1</sub> , $\vec{t}_x$ , $\vec{t}_y$ , $\vec{t}_z$	Landmark for the frame of reference secured to the tibia
R <sub>S</sub> (S <sub>1</sub> , $\vec{s}_x$ , $\vec{s}_y$ , $\vec{s}_z$ )	Landmark for the frame of reference secured to the sensor
R <sub>N</sub> (O <sub>N</sub> , $\vec{n}_x$ , $\vec{n}_y$ , $\vec{n}_z$ )	Landmark for the frame of reference of the navigator
Anatomic landmark points	
R <sub>F</sub> $\vec{f}_1$ , $\vec{f}_2$ , $\vec{f}_3$	Femoral anatomic landmark
T $\vec{t}_1$ , $\vec{t}_2$ , $\vec{t}_3$	Tibial anatomic landmark
N <sub>T</sub> , X <sub>F</sub> , X <sub>T</sub> , Z <sub>F</sub> , Z <sub>T</sub>	
<sup>a</sup> Cinematic acquisition method.	
<sup>b</sup> Acquisition method using the ballpoint of the navigator sensor.	

**Table 1b**

Geometric features (in mm) of the femur and tibia.

Length of femur	468
C <sub>M</sub> C <sub>L</sub> distance	60
Length of tibia	401
M <sub>1</sub> M <sub>2</sub> distance	56
S <sub>1</sub> S <sub>2</sub> distance	150

## 2.5. Simulation using the Monte Carlo statistical method

To model the inaccuracy, the coordinates of the reflective optical tracker centres and acquisition anatomic points were distributed within spheres of uncertainty, whose dispersion diameters were specific of each of these points (Table 2). Pseudo-random values were generated using the Mersenne Twister<sup>1</sup> algorithm to

<sup>1</sup> A pseudo-random number generator is an algorithm that generates a number sequence exhibiting some of the properties of randomness. Among these

ensure equi-probable sampling of the points within the uncertainty sphere. The variation of the infrared optical measurement system was selected within a diameter range of 0 to 1 mm. For each palpated anatomic point, the coordinates of the centres of the three optical sensors (S<sub>1</sub>, S<sub>2</sub>, S<sub>3</sub>) of the digital localising system and those of the three optical sensors (T<sub>1</sub>, T<sub>2</sub>, T<sub>3</sub>) of the reference frames for the tibia or femur (F<sub>1</sub>, F<sub>2</sub>, F<sub>3</sub>) were simulated. First, the coordinates of the six reflective optical points were used to compute each anatomic point. These same points were then distributed in random positions, to assess the impact of infrared optical system variability on the accuracy of the constructed skeletal landmarks. Then, the anatomic points were dispersed, in turn, to combine the variability of the 3D optical measurement system with the lack of reproducibility of the acquisition points.

## 2.6. Variability of the anatomic points

The alpha, beta, and gamma rotations around the z, x, and y axes, respectively, of the anatomic frames of reference express the inaccuracy of the 3D orientation of the prosthetic components in flexion-extension, valgus-varus, and rotation, respectively.

The 3D discrepancies between the femoral and tibial landmarks were each projected on the appropriate femoral anatomic plane, to interpret the alignment of the lower limb equipped with the prosthesis. A descriptive statistical analysis was performed on 30,000 simulations, each of which allowed extraction of the angle parameters **a**, **b**, and **g**. The set of uncertainties of these angles was derived from these 30,000 values at 3SDs.

## 3. Results

Each **a**, **b**, and **g** error for the femoral frame of reference R<sub>F</sub> (Fig. 4) followed a linear progression despite the multidirectional nature of the randomly generated point positions. Virtual implantation of the femoral implant showed maximal errors and variation ranges of 1.65° (±1.15°) in flexion-extension, 1.51° (±1.44°) in valgus-varus, and 2.37° (±2.37°) in axial rotation. In the most extreme case, when all the tibial anatomic points varied within the maximal uncertainty range, the maximal angle errors for the tibial frame of reference were 0.9° in flexion-extension, 0.98° in valgus-varus, and 3.84° in axial rotation (Fig. 5). The values of the tibio-femoral angles were expressed after simulation according to the dispersion of the infrared measurement system combined or not combined with the dispersion of the anatomic points (Tables 3 and 4).

## 4. Discussion

### 4.1. Main study findings and limitations

Based on the uncertainties related to the measurement system and anatomic point acquisition, the femoral and tibial frames of reference exhibited maximal errors in rotation **a** (flexion-extension), **b** (valgus-varus), and **g** (axial rotation) of 1.65° (0.9°), 1.51° (0.98°), and 2.37° (3.84°), respectively. The effects of these errors on the coronal, sagittal, and rotational tibio-femoral angles were 0.92°,

algorithms, the Mersenne Twister, developed in 1997 by Makoto Matsumoto and Takuji Nishimura, is recognised as producing high-quality and robust pseudo-random numbers. The Monte Carlo statistical methods (thus named by analogy with games of chance played in Monte Carlo casinos) was developed in 1947 by Nicholas Metropolis. A pseudo-random number generator is used to obtain a number of values so large that it represents all possible measurement scenarios, according to a probabilistic technique. A descriptive statistical analysis performed after a Monte Carlo simulation provides an interpretation of the behaviour of the system under study.

**Table 2**

Parameters for dispersion of the points used to construct the skeletal landmarks.

Acquisition points for the skeletal landmarks		Acquisition method	Dispersion at the diameter (mm)	Comment	References
Centre of hip	H	Cinematic acquisition method	3	Precision algorithm	Siston, Picard
Centre of distal femoral epiphysis	N	Manual localisation 1 cm above the top of the anterior notch at the level of the depth of the trochlea	7	This anatomic zone is very easily identified after surgical exposure	∅
Tips of the two posterior condyles	C <sub>L</sub> and C <sub>P</sub>	Acquisition from a cloud of points obtained by surface digitisation of the two posterior condyles	2	The algorithm determines the two tips of the posterior condyles relative to the mechanical axis of the femur	Perrin
Centre of proximal tibial epiphysis	S	Manual localisation of the posterior part of the anterior pre-spinal surface	6	This anatomic zone is clearly flanked by the two tibial spines.	∅
Sagittal tibial vector	S <sub>1</sub> S <sub>2</sub>	Positioning of the navigator sensor, which materialises the orientation of the vector X <sub>T</sub>	15	Risk of poor sensor positioning. Involves several anatomic landmarks within the field of view	∅
Medial malleolus	M <sub>M</sub>	Manual localisation at the middle of the medial edge of the medial malleolus	4	Palpation of both malleoli. The algorithm compensates for the errors and calculates the location of the centre of the ankle	Siston
Lateral malleolus	M <sub>L</sub>	Manual localisation at the middle of the lateral edge of the lateral malleolus	6		

1.13°, and 4.24° respectively. Our hypothesis that navigation systems result in non-negligible errors related to lack of accuracy of the optical system and of the surgeon when palpating the anatomic points was confirmed by the numerical simulation study, most

**Table 3**

Imprecision expanded to three standard deviations of the tibio-femoral angles expressed in degrees according to dispersion of the optical measurement system in millimetres.

Optical measurement system (mm)	Flexion-Extension (°)	Valgus-varus (°)	Axial rotation (°)
0.1	0.0	0.0	0.2
0.2	0.0	0.1	0.3
0.3	0.1	0.1	0.4
0.4	0.1	0.1	0.6
0.5	0.1	0.2	0.8
0.6	0.1	0.2	0.9
0.7	0.2	0.2	1.0
0.8	0.2	0.3	1.2
0.9	0.2	0.3	1.4
1	0.2	0.3	1.5

**Table 4**

Imprecision within the 99.7% confidence interval of the tibio-femoral angles expressed in degrees, according to dispersion of surgeon localisations combined with measurement system variability. The infrared optical system and anatomic points varied gradually within their specific uncertainty zones, which ranged across points from 1 to 15 mm. Each anatomic point was limited to its maximal uncertainty variation. Maximum measurement system dispersion was set at 1 mm at the diameter.

Optical measurement system and surgeon (mm)	Flexion-Extension (°)	Valgus-varus (°)	Axial rotation (°)
1	0.4	0.4	1.6
2	0.6	0.7	1.8
3	0.8	1.0	1.9
4	0.8	1.0	2.0
5	0.9	1.1	2.2
6	0.9	1.1	2.4
7	0.9	1.1	2.5
8	0.9	1.1	2.7
9	0.9	1.1	2.9
10	0.9	1.1	3.1
11	0.9	1.1	3.3
12	0.9	1.1	3.6
13	0.9	1.1	3.8
14	0.9	1.1	4.0
15	0.9	1.1	4.2

notably regarding the deviations in rotation. The variability of the infrared optical measurement system had a limited impact on the tibio-femoral alignment angles, with a maximal error of 1.49° in the horizontal plane. For our study, we assumed a strong connection between the two rigid bodies and the femoral or tibial skeleton, which was assumed to have no deformability. Nevertheless, secondary displacement of the reference frame can occur during an inadvertent movement of the surgeon or in patients with osteoporosis and may result in an unnoticed error [19]. In addition, our navigation simulator did not take into account errors related to bone quality or to the precision of the oscillating saw blade guided into the slot of the cutting block. Plaskos et al. [20] reported that saw blade bending or inadequate cutting guide fixation could result in cutting errors that could be detected by applying a tracking plate onto the bone cuts. Nevertheless, the incorporation at the initial step of an excessively large number of errors of different levels might result in a more global and less relevant analysis of the results.

#### 4.2. Variability of the 3D optimal measurement system on alignment of the limb equipped with the prosthesis

Commercially available infrared optimal measurement systems are described by their manufacturers as having a resolution of about 0.10 mm. However, interference with light in the operating room [17,21] may adversely affect the infrared optical signal and the measurements of the spatial coordinates of the reflective trackers. In our study, with 1 mm of dispersion of the reflective infrared trackers, the optical measurement system resulted in lower-limb alignment errors of 1.5° in rotation and less than 0.5° in the coronal plane. Thus, the 3D optical measurement system is not the main explanation to the anatomical landmark variability evidenced in our study with combined dispersion.

#### 4.3. Impact of anatomical point dispersion on accuracy of skeletal landmark registration

Yau et al. performed a cadaver study to assess intra- and inter-observer variability of anatomic points used for navigation-assisted TKA [22]. The error in rotation around the trans-epicondylar axis was 9.1°. A computed tomography study by Galaud et al. [23] showed poor reproducibility of using the epicondyles to define femoral rotation during navigation-assisted TKA. To identify the tips of the two femoral condyles, we considered a series of

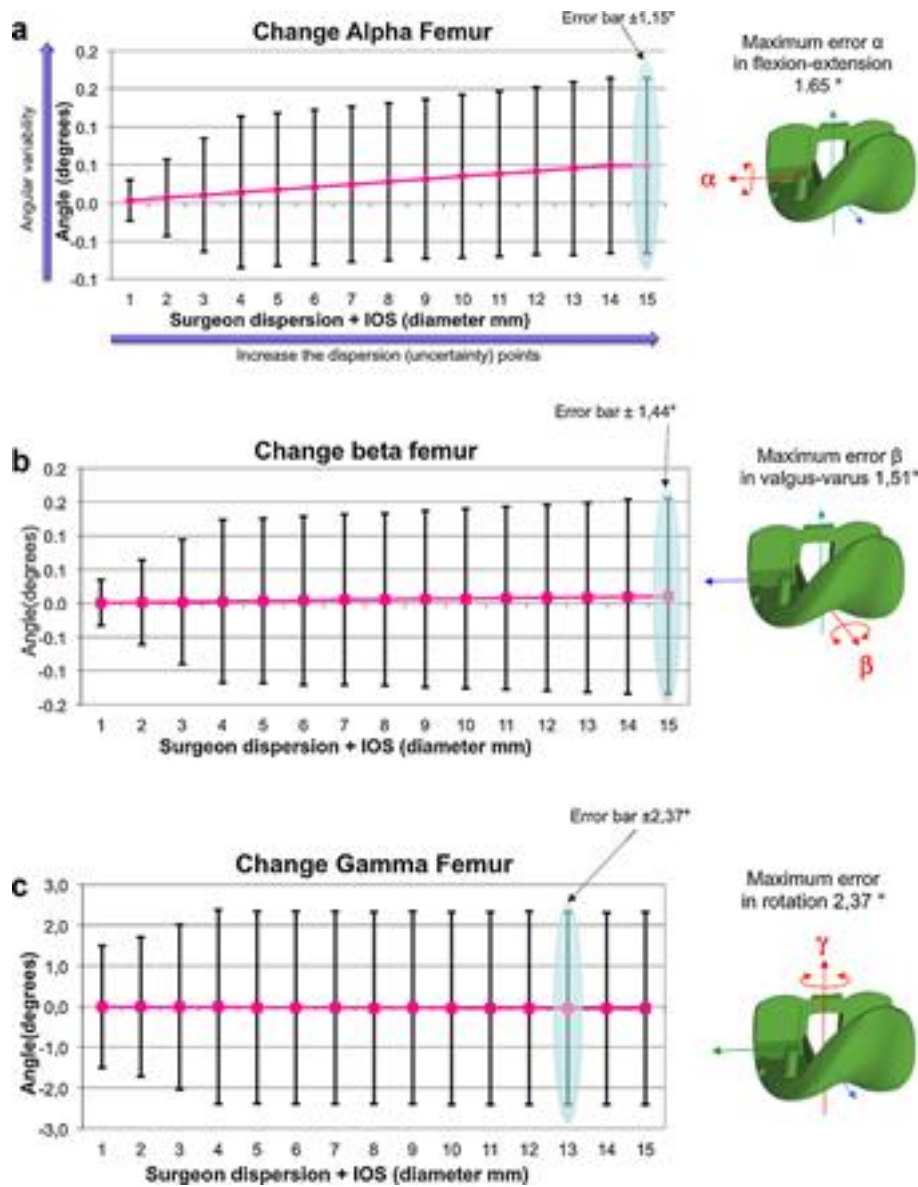


**Fig. 4.** Assessment of variability of the  $R_T$  femoral landmark according to dispersion of the infrared optical system (IOS) and acquisition of the anatomic points. The variation related to the 3D infrared optical measurement system was propagated within a range of 0 to 1 mm in diameter. The diameter of acquisition point dispersion increased to its own specific maximal value. a, b and c: progression of errors  $\alpha$  (flexion-extension),  $\beta$  (varus-valgus), and  $\gamma$  (rotation), respectively 3DMM, 3D measurement machine.

surface points from the posterior condylar region. Using an algorithm to treat point clusters considerably improves precision compared to freehand localization [24]. This fact explains the differences between our findings and the results of the experiments reported by Yau et al. [25]. For the tibia, rotation error related to inadequate positioning of the  $\bar{X}_T$  vector may generate an oblique plane effect on the tibial bone cut, which adversely affects alignment of the tibial component in the coronal plane. According to Dejour et al. [26], with  $7^\circ$  of tibial slope, a  $20^\circ$  positioning error in rotation of the tibial component adds  $2^\circ$  of varus to the tibial implant. After simulation, the tibial frame of reference  $R_T$  exhibited nearly  $\pm 4^\circ$  of axial rotation variability. Clearly, freehand digital registration of the sagittal tibial axis is a weak link in the chain of skeletal landmark acquisition during navigation-assisted TKA. The posterior edge of the two tibial plateaux, anterior tibial crest, centre of the ankle, and axis of the second metatarsal constitute a constellation of anatomic landmarks present at various levels within the field of view of the surgeon.

#### 4.4. Comparison with clinical studies of computer-aided TKA

Our results are difficult to compare with those of previously published clinical studies. Nevertheless, in agreement with the two meta-analyses recently published by Fu et al. [14] and Cheng et al. [13], our virtual navigation system was robust for controlling alignment in the coronal plane. Thus, the error in varus-valgus of the tibio-femoral mechanical axis did not exceed  $1.5^\circ$ . The long mechanical axes are far less vulnerable to variability in constitutive anatomic points compared to the shorter rotational epiphyseal axes. For a femoral mechanical axis of about 40 cm in length, a 1-cm error at one end results according to a simple trigonometric analysis in an error of  $0.57^\circ$ . In contrast, the error is  $5.7^\circ$  for a trans-epicondylar axis measuring 10 cm in length. The results obtained using our modelling approach confirm these data indicating greater vulnerability of navigating systems in rotation. Rotational errors in TKA implanted using navigation were indisputably underestimated in recently published studies [15,16,27], in which prosthesis alignment was assessed based only on standard radiographs.

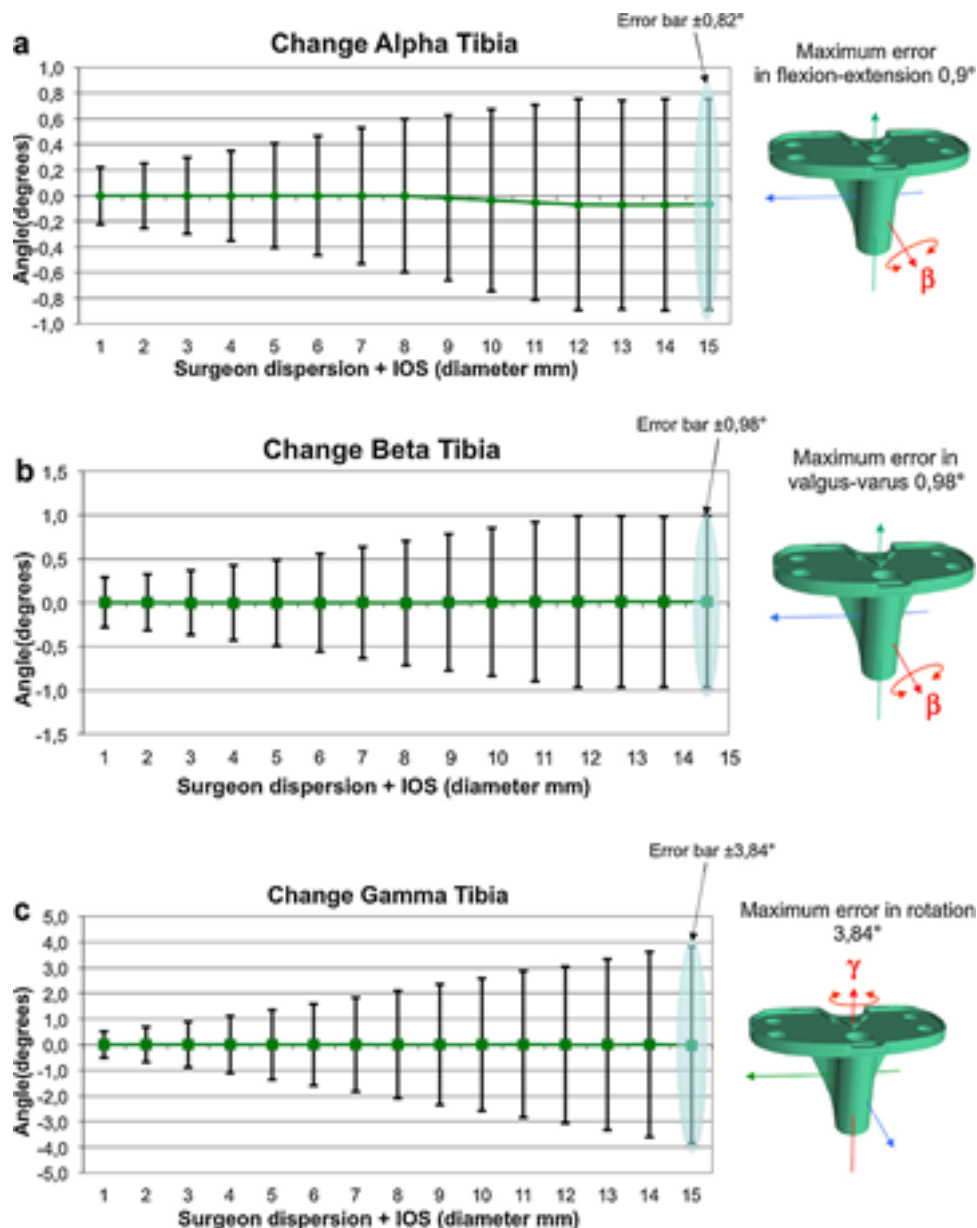


**Fig. 5.** Changes in variability of the tibial landmark  $R_T$  according to dispersions of the infrared optical system (IOS) and surgeon. a, b and c: progression of error a (flexion-extension), b (varus-valgus), and g (rotation), respectively.

## 5. Conclusion

Our original study involving the development of a virtual TKA navigator followed by error simulation established that variability in the infrared optical measurement system has only negligible effects on the accuracy of the anatomic landmark registration. In contrast, adding dispersion of the acquisition anatomic points adversely affects the reliability of these same landmarks for guiding rotational positioning, without affecting the quality of implant alignment in the frontal and sagittal planes, supporting the relevance of the numerical data used to guide the surgical procedure.

## Disclosure of interest

The authors declare that they have no conflicts of interest concerning this article.

## Appendix A. Supplementary data

## References

- [1] Jung WH, Chun CW, Lee JH, Ha JH, Jeong JH. The accuracy of the extramedullary and intramedullary femoral alignment system in total knee arthroplasty for varus osteoarthritic knee. *Knee Surg Sports Traumatol Arthrosc* 2013;21:629–35.
- [2] Iorio R, Bolle G, Conteduca F, Valeo L, Conteduca J, Mazza D, et al. Accuracy of manual instrumentation of tibial cutting guide in total knee arthroplasty. *Knee Surg Sports Traumatol Arthrosc* 2013;21:2296–300.
- [3] Lerat JL, Besse JL, Desme D, Kadi S, Chouteau J, Rollier JC, et al. Accuracy of total knee replacement bone cuts using a conventional ancillary system: 300 Innex total knee arthroplasties. *Rev Chir Orthop Reparatrice Appar Mot* 2006;92:248–56.
- [4] Reed SC, Gollish J. The accuracy of femoral intramedullary guides in total knee arthroplasty. *J Arthroplasty* 1997;12:677–82.
- [5] Lustig S, Scholes CJ, Oussedik SI, Kinzel V, Coolican MR, Parker DA. Unsatisfactory accuracy as determined by computer navigation of VISIONAIRE



- patient-specific instrumentation for total knee arthroplasty. *J Arthroplasty* 2013;28:469–73.
- [6] Barrack RL, Ruh EL, Williams BM, Ford AD, Foreman K, Nunley RM. Patient specific cutting blocks are currently of no proven value. *J Bone Joint Surg Br* 2012;94(11 Suppl. A):95–9.
- [7] Conteduca F, Iorio R, Mazza D, Caperna L, Bolle G, Argento G, et al. Evaluation of the accuracy of a patient-specific instrumentation by navigation. *Knee Surg Sports Traumatol Arthrosc* 2013;21:2194–9.
- [8] Nunley RM, Ellison BS, Zhu J, Ruh EL, Howell SM, Barrack RL. Do patient-specific guides improve coronal alignment in total knee arthroplasty? *Clin Orthop Relat Res* 2012;470:895–902.
- [9] Stronach BM, Pelt CE, Erickson J, Peters CL. Patient-specific total knee arthroplasty required frequent surgeon-directed changes. *Clin Orthop Relat Res* 2012;470:895–902.
- [10] Bathis H, Perlick L, Tingart M, Luring C, Zurakowski D, Grifka J. Alignment in total knee arthroplasty. A comparison of computer-assisted surgery with the conventional technique. *J Bone Joint Surg Br* 2004;86:682–7.
- [11] Bauwens K, Matthes G, Wich M, Gebhard F, Hanson B, Ekkernkamp A, et al. Navigated total knee replacement. A meta-analysis. *J Bone Joint Surg Am* 2007;89:261–9.
- [12] Brin YS, Nikolaou VS, Joseph L, Zukor DJ, Antoniou J. Imageless computer assisted versus conventional total knee replacement. A Bayesian meta-analysis of 23 comparative studies. *Int Orthop* 2011;35:331–9.
- [13] Cheng T, Zhao S, Peng X, Zhang X. Does computer-assisted surgery improve postoperative leg alignment and implant positioning following total knee arthroplasty? A meta-analysis of randomized controlled trials. *Knee Surg Sports Traumatol Arthrosc* 2012;20:1307–22.
- [14] Fu Y, Wang M, Liu Y, Fu Q. Alignment outcomes in navigated total knee arthroplasty: a meta-analysis. *Knee Surg Sports Traumatol Arthrosc* 2012;20:1075–82.
- [15] Hetaimish BM, Khan MM, Simunovic N, Al-Harbi HH, Bhandari M, Zalzal PK. Meta-analysis of navigation vs conventional total knee arthroplasty. *J Arthroplasty* 2012;27:1177–82.
- [16] Mason JB, Fehring TK, Estok R, Banel D, Fahrback K. Meta-analysis of alignment outcomes in computer-assisted total knee arthroplasty surgery. *J Arthroplasty* 2007;22:1097–106.
- [17] Song EK, Seon JK, Park SJ, Yoon TR. Accuracy of navigation: a comparative study of infrared optical and electromagnetic navigation. *Orthopedics* 2008;31 (10 Suppl. 1).
- [18] Brin YS, Livshetz I, Antoniou J, Greenberg-Dotan S, Zukor DJ. Precise landmarking in computer assisted total knee arthroplasty is critical to final alignment. *J Orthop Res* 2010;28:1355–9.
- [19] Lee DH, Padhy D, Lee SH, Nha KW, Park JH, Han SB. Osteoporosis affects component positioning in computer navigation-assisted total knee arthroplasty. *Knee* 2012;19:203–7.
- [20] Plaskos C, Hodgson AJ, Inkpen K, McGraw RW. Bone cutting errors in total knee arthroplasty. *J Arthroplasty* 2002;17:698–705.
- [21] Lionberger DR, Weise J, Ho DM, Haddad JL. How does electromagnetic navigation stack up against infrared navigation in minimally invasive total knee arthroplasties? *J Arthroplasty* 2008;23:573–80.
- [22] Yau WP, Leung A, Liu KG, Yan CH, Wong LL, Chiu KY. Interobserver and intraobserver errors in obtaining visually selected anatomical landmarks during registration process in non-image-based navigation-assisted total knee arthroplasty. *J Arthroplasty* 2007;22:1150–61.
- [23] Galaud B, Beaufile P, Michaut M, Abadie P, Fallet L, Boisrenoult P. Distal femoral torsion: comparison of CT scan and intra operative navigation measurements during total knee arthroplasty. A report of 70 cases. *Rev Chir Orthop Reparatrice Appar Mot* 2008;94:573–9.
- [24] Perrin N, Stindel E, Roux C. BoneMorphing versus freehand localization of anatomical landmarks: consequences for the reproducibility of implant positioning in total knee arthroplasty. *Comput Aided Surg* 2005;10:301–9.
- [25] Yau WP, Leung A, Chiu KY, Tang WM, Ng TP. Intraobserver errors in obtaining visually selected anatomic landmarks during registration process in nonimage-based navigation-assisted total knee arthroplasty: a cadaveric experiment. *J Arthroplasty* 2005;20:591–601.
- [26] Dejour D, Tabutin J, Chambat P. Les coupes osseuses : tibiale, fémorale, rotulienne. 9<sup>èmes</sup> Journées lyonnaises de chirurgie du genou et de l'épaule, 8, 9, 10 avril 1999. p. 9–20.
- [27] Tingart M, Luring C, Bathis H, Beckmann J, Grifka J, Perlick L. Computer-assisted total knee arthroplasty versus the conventional technique: how precise is navigation in clinical routine? *Knee Surg Sports Traumatol Arthrosc* 2008;16:44–50.